Journal of Hydrology 635 (2024) 131081

Contents lists available at ScienceDirect

Journal of Hydrology

journal homepage: www.elsevier.com/locate/jhydrol

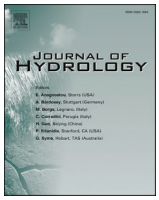

Research papers

The impact of deep glacial water diversions from a hydroelectric reservoir in the thermal dynamics of a sub-arctic lake

Cintia L. Ramón [a,*], Francisco J. Rueda [a], Morgane C. Priet-Mahéo [b], Hrund Andradóttir [c]

[a] Department of Civil Engineering and Water Institute, University of Granada, Granada, Spain
[b] Icelandic Meteorological Office, Reykjavík, Iceland
[c] Faculty of Civil and Environmental Engineering, University of Iceland, Reykjavík, Iceland

ARTICLE INFO

Keywords:
Hydroelectric project
Water diversion
Sub-arctic lake
Impact assessment
Thermal dynamics
Water-column stability

ABSTRACT

Interbasin water diversions associated with hydroelectric power operations can influence the physics and water quality of downstream receptor lakes. Little is known about the impact of such diversions in sub-arctic and arctic lakes, which are characterized by weak summer stratification and a high relative contribution of cold and highly turbid tributaries of glacial origin. From 2003 to 2007, Lake Lagarfljót (53 km^2, 65°N) experienced a series of changes in its natural hydrological conditions as part of the 690 MW Kárahnjúkar hydroelectric project. The most significant change was the damming and diversion of a second glacial river into the lake, reducing its hydraulic residence time by a factor of three, and increasing its background turbidity levels by one order of magnitude. Here we developed a three-dimensional hydrodynamic modeling approach to assess the impacts of this project on the Lake's physics. We accounted for the uncertainty in pre-dam suspended-solids data and conducted a stepwise assessment of each alteration in the hydrological forcing and lake background conditions. The results revealed abrupt changes in the lake's summer thermal dynamics. Advective heat fluxes now have a similar magnitude to atmospheric heat exchanges or even dominate the lake's heat balance during the second half of the thermal stratification period. The diversion of deep water from Hálslón reservoir led to a net cooling of both the surface (median ≈1°C) and deep (median ≈0.6 °C) layers of the lake during the thermal stratification period, to a ≈ 45 % decrease in the average summer water column Schmidt stability and a two-week decrease in the duration of the thermal stratification period. The lower stability of the water column and deep river-plume intrusions now facilitate nearly complete hypolimnetic water renewal during the thermal stratification period. The proposed modeling approach, which deconstructs the lake's conditions from post- to pre-operational stages, is suitable for lakes with limited pre-operational in-situ data.

1. Introduction

Hydropower, being one of the oldest renewable sources, has the potential to play an important role in the world's energy transition during climate change (e.g., Denton et al., 2022). However, concerns have arisen regarding the potential negative impacts of reservoir storage and release practices on downstream water quantity, water quality and the ecosystems dependent on downstream water (e.g., Maavara et al., 2020; Winton et al., 2019; Zhang et al., 2020), which has slowed down the implementation of hydropower projects. Dams have been observed to cause physical changes in downstream rivers and lakes, including alterations in the flow (Anselmetti et al., 2007; Dai et al., 2008; Loizeau and Dominik, 2000) and thermal (e.g., Lessard and Hayes, 2003; Prats et al., 2010; Preece and Jones, 2002) regimes, as well as, reductions in sediment transport (e.g., Anselmetti et al., 2007; Finger et al., 2006; Loizeau and Dominik, 2000; Yang et al., 2007). These hydrological changes can have negative implications for the water quality of downstream lakes. For instance, the moderation of peak particle fluxes and flow rates by dams can decrease the frequency of deep intrusions of rivers into downstream lakes, leading to increased particle and nutrient supply to the surface layers (e.g., Finger et al., 2006; Loizeau and Dominik, 2000), and/or to a decrease in deep-water renewal and re-oxygenation (e.g., Fink et al., 2016; Wüest et al., 1988). It is important to note that the impacts of dams can extend beyond the immediate river catchment where they are located if, for example, water diverted from dammed reservoirs is not returned to the same river but transferred

* Corresponding author.
E-mail addresses: crcasanas@ugr.es (C.L. Ramón), fjrueda@ugr.es (F.J. Rueda), hrund@hi.is (H. Andradóttir).

https://doi.org/10.1016/j.jhydrol.2024.131081
Received 13 July 2023; Received in revised form 10 February 2024; Accepted 29 February 2024
Available online 28 March 2024

to another river or lake. In that case, the outflows from the power plant may have different physical–chemical characteristics compared to the receiving streams (Bonalumi et al., 2012, 2011). Depending on the magnitude of diverted water relative to the natural tributaries entering the lake (e.g., Bonalumi et al., 2012, 2011), this could lead to changes in the natural forcing of lakes and, thus, to changes in their flow and stratification regime (e.g., Bermúdez et al., 2018).

Most of the knowledge gained about the impact of water diversions is related to pumped-storage hydroelectric projects or water-diversion projects that aim to improve the water quality of the receptor stream in temperate lakes (e.g., Bonalumi et al., 2012, 2011; Chen et al., 2016; Kobler et al., 2018; Zhang and Wu, 2020). However, to the best of our knowledge, few or no studies have evaluated the impact of high-magnitude water diversions in lakes close to or above the Arctic Circle. Glacial water systems differ from their more temperate counterparts due to their low temperature and high sediment content, weak summer stratification and inflow intrusions developing at a wide range of depths (e.g., Priet-Mahéo et al., 2019; Ramón et al., 2020). Resolving the internal dynamics of such systems thus requires a high temporal resolution of hydrometeorological forcing, including that of riverine sediments, which can drastically vary both during short (e.g., discharge event) and long (seasonal) timescales.

An example of a high-magnitude interbasin transfer is occurring under the Kárahnjúkar Hydroelectric Project in NE Iceland (hereon, the Project). The Project involved the damming and interconnection of two separate glacial rivers (Jökulsá a Dal and Jökulsá í Fljótsdal), which originate in the Vatnajökull glacier —the largest glacier of Europe—, their convergence upstream of Lake Lagarfljót, and their entrance into the lake in its southern end (Fig. 1). This project, the largest in Icelandic construction history with a total cost of 2 billion USD, has influenced the flux of most dissolved elements towards the ocean (Eiriksdottir et al., 2017). There is also evidence that the net primary production and freshwater char stocks in Lake Lagarfljót have decreased after the Project due to an increase in the turbidity of the lake (Eiriksdottir et al., 2017 and reference therein). However, despite the primary controlling role of temperature in lake geochemical and ecological processes (e.g.,

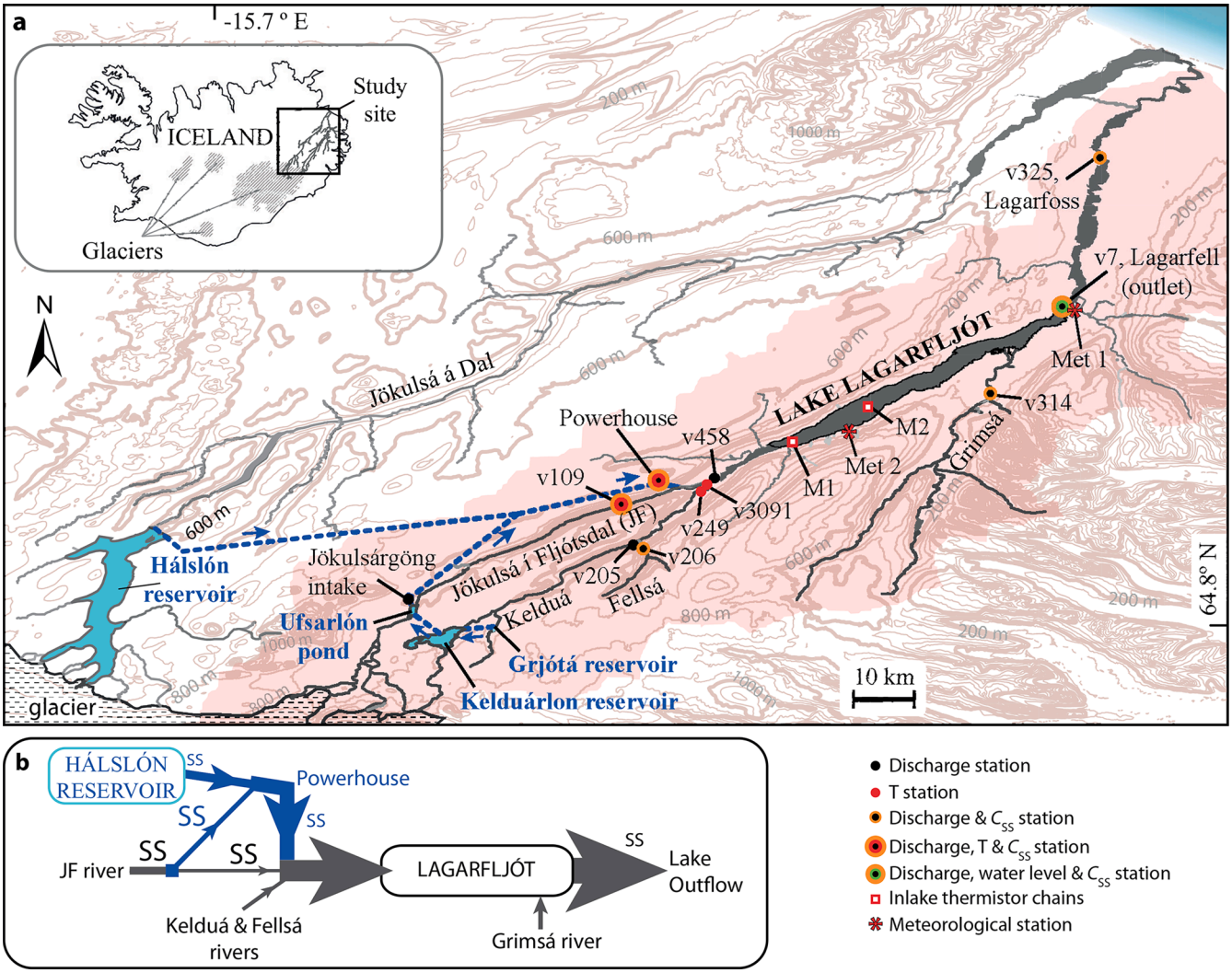

Fig. 1. Lake Lagarfljót, its major tributaries, and the Kárahnjúkar Hydroelectric Scheme. (a) Waterways in the Jökulsá í Fljótsdal and Jökulsá á Dal river basins. The red-shaded area marks the natural basin of the JF river. Dots indicate the locations of Q/T/SS/water level stations (see details in Table S1), asterisks show the location of the two meteorological stations and squares represent the locations of thermistor chains M1 and M2 deployed in the lake. The dotted blue lines indicate the approximate location of the subterranean tunnels of the Kárahnjúkar Hydroelectric Scheme and blue arrows show the main direction of the flow in those tunnels. Light-brown lines depict isohypses at intervals of 100 m. Thicker lines denote elevations of 200, 600, and 1000 m above sea level (b) Schematic of the flow path into and out of the lake. Arrows indicate the flow path and their size is proportional to the magnitude of the discharge. Pathways contributing with suspended solids are marked with the letters SS, and their size is proportional to the concentration of suspended solids. The new reservoirs, ponds, and pathways introduced as part of the Kárahnjúkar Hydroelectric Scheme are indicated in blue in (a-b). (For interpretation of the references to colour in this figure legend, the reader is referred to the web version of this article.)

De Senerpont Domis et al., 2013; Wetzel, 2001), the effect of the Project on the heat balance of the lake, the length and strength of the summer stratification, and, in general, the thermal dynamics of Lake Lagarfljót remains unknown. The goal of this research was to assess the impacts of the Project on the natural forcings of Lake Lagarfljót (river discharges, temperatures, and suspended solid concentrations) and how these changes have affected the thermal dynamics of the lake during the summer stratification period. A two-pronged approach was taken. Firstly, the historical data was evaluated to detect which hydrometeorological variables were most affected by the Project. Secondly, given the rather limited set of in-lake measurements before the Project, we used a three-dimensional hydrodynamic model to reproduce the lake conditions before and after the Project and disentangle the effect of each change introduced by the Project in the lake catchment. Specifically, the model was used to assess the effect of damming and river water diversion on (1) the lake's heat balance, (2) the strength and duration of the density stratification and its connection with (3) the dynamics of the river intrusion depths, and (4) the amount of deep-water renewal.

2. Study site and field measuring stations

Lake Lagarfljót (65.1°N, −14.6°E) is one of Iceland's largest natural lakes, with a surface area of 53 km^2 and 2.7 × 10^9 m^3 storage volume. It includes a 20 km long parabolic deep S-basin, with a maximum depth of 110 m, joined to a 7 km long, shallow shelf (N-basin), with a maximum depth of 42 m. The main historical drainage to Lake Lagarfljót was the glacial river Jökulsá í Fljótsdal (hereafter, JF; Fig. 1), with highly seasonal flow rates and suspended sediment loads. Nearby, the non-glacial rivers Kelduá and Fellsá converge with the JF river 9 km upstream of the lake entrance (Fig. 1). The major non-glacial tributary, though, is river Grimsá that enters the shallower N-basin before the single outlet of the lake at Lagarfell.

In 2003–2007, the catchment of Lake Lagarfljót underwent a series of transformations as part of the 690 MW Kárahnjúkar Hydroelectric Project, which is owned and operated by Landsvirkjun, the National Power Company of Iceland. The Jökulsá á Dal river was dammed, creating the Hálslón reservoir (Fig. 1) of similar size as Lake Lagarfljót (57 km^2, 2.1 × 10^9 m^3 max. storage; Aðalsteinsson, 2017). Additionally, three interconnected smaller reservoirs with a total storage capacity of 0.2 × 10^9 m^3 were constructed: Grjótá reservoir and the largest 8-km^2 Kelduárlón reservoir in the watershed of river Kelduá, and the 1-km^2 Ufsarlón pond damming JF (Fig. 1). Water from Hálslón reservoir is conveyed to the power plant from a deep intake (90-m deep at full supply level) through a nearly 40-km long headrace tunnel (see dotted-blue lines in Fig. 1a), and water from Ufsarlón pond is conveyed from its near-surface intake through the 13.3-km long Jökulsá tunnel, which connects to the headrace tunnel approximately at its midpoint (Fig. 1a). The Kárahnjúkar Power plant became operational in November 2007 and fully operational in March 2008. Its outflow converges into the JF river at approximately 100 m upstream of its confluence with the Kelduá river (Fig. 1a). The outflow from the power plant is almost constant through the year (116 ± 17 m^3/s).

Daily or hourly continuous records for the period 1995–2016 of discharges and water temperature for the main tributaries to the lake, the powerhouse and the lake outflow were made available through the Icelandic Meteorological Office (IMO), Landsvirkjun and the Orkusalan electrical company. Water samples for suspended solid analyses were collected discretely in the different tributaries, approximately 8–14 times per year. Details of measuring sites and available data are shown in Fig. 1a (details in Text S1 and Table S1 in the Supporting Information). From 2000 to 2015 — covering the period before and after the Project — Landsvirkjun deployed from mid-May to December, a thermistor chain with four Starmon Mini thermistors (accuracy: 0.1 °C) measuring hourly at 1.5, 16, 31, and 42 m at a ≈ 50 m deep location near the southern end of the lake (mooring M1, Fig. 1a). A second thermistor chain, measuring hourly with at least a common vertical resolution at 1,10, 20, 30, 40, 50 and 100 m, was deployed at the deepest location of the lake (mooring M2, Fig. 1a) in the post-dam period from 2009 to 2014.

3. Historical data analyses

Our modeling approach is grounded in the analysis of the available historical hydrometeorological data. Therefore, for the sake of clarity, we present the results of analyzing the available hydro-meteorological data covering the period 1995 to 2016 upfront. Three are the sources of the southern inflow into the lake: the outflows from the Kárahnjúkar power plant, the glacial JF river and the non-glacial Kelduá-Fellsá river. We assumed that these three sources were completely mixed by the time they entered the lake, approximately 9 km downstream from their confluence (Fig. 1). The temperature and suspended sediment concentration of the southern inflow were calculated as the volumetric weighted average of the three confluent streams (for details on handling sparse data sets, see Section 4.3.1). To detect linear trends, we calculated Sen slopes (e.g., O'Reilly et al., 2015) and their significance was evaluated using a Z-test (Burkey, 2023). We also identified abrupt changes in the hydrological signals around the time the power plant became operational by employing the Bayesian ensemble algorithm called BEAST, developed by Zhao et al. (2019). BEAST considers that a time series can be composed of seasonality, trend, abrupt changes, and noise. It utilizes linear models to detect the seasonal and trend signals where abrupt changepoints are included as unknown parameters. Bayesian inference is used to explicitly address model uncertainties.

Changepoints were detected in the underlying trend or seasonal signals of almost all hydrological variables in the southern inflows and outflows of Lake Lagarfljót late 2007 or early 2008 (vertical lines in Fig. 2; see also Fig. S2). Firstly, the annual outflows increased from 59 m^3/s to 158 m^3/s after the Project (Fig. 2a). The average hydraulic residence time of water in the lake has, therefore, decreased by a factor of ≈ three, from 1.4 to 0.5 years. Given the approximately constant through-time discharges of the power plant, the shape of the seasonal discharge signal has not changed after the Project (no seasonal changepoint detected in Fig. 2a), with maximum discharges taking place around June and minimum discharges occurring in winter. But this also means that the southern inflow discharges have increased in winter from almost zero to 110 m^3/s after the dam. The average water level of the lake has increased by ≈10 cm (from 20.47 to 20.57 m.a.s.l) without a changepoint in its seasonal variability (Fig. 2b).

The seasonal cycle of suspended solid concentration C_{SS} in the southern inflows was characterized before the dam by an almost zero particle input until the warm season and maximum values during the summer (Fig. 2c). As a result of the Project, C_{SS} has increased during the cold season from almost 0 to an average of ≈182 mg L^{-1} in Dec-Feb. The magnitude of the C_{SS} peaks in the warm season, in turn, has decreased (by ~ 170 mg L^{-1} for Jul-Sep, Fig. 2c). The lake remains now highly turbid even in winter, and C_{SS} in the lake outflow is now one order of magnitude higher than were before (from O(1 0^1) to O(1 0^2) mg L^{-1}) (see changepoint in Fig. 2c).

Mean annual water temperatures have decreased by ≈ 1 °C and ≈ 0.5 °C in lake inflows and outflow after damming (Fig. 2d). This cooling is caused by the outflows from the powerhouse which peak at only 6 °C in summer. This is because of the construction of the 200-m deep Hálslón reservoir, which tends to have colder water than the JF river (Fig. S1), to the deep intake in Hálslón reservoir, and to the transport in subterranean tunnels with no atmospheric heating. If we focus on summer months, here taken as July to September, indeed significant cooling was observed in the southern inflow water temperature (Table 1, Fig. S2). Of the three water masses that mix to form the southern inflow to the lake, only the powerhouse could be responsible for this observed cooling, since (1) the JF river temperature upstream of the power plant warmed, which can be explained by significantly lower discharge (and water depth, Table 1); (2) Kelduá water temperature decreased but not

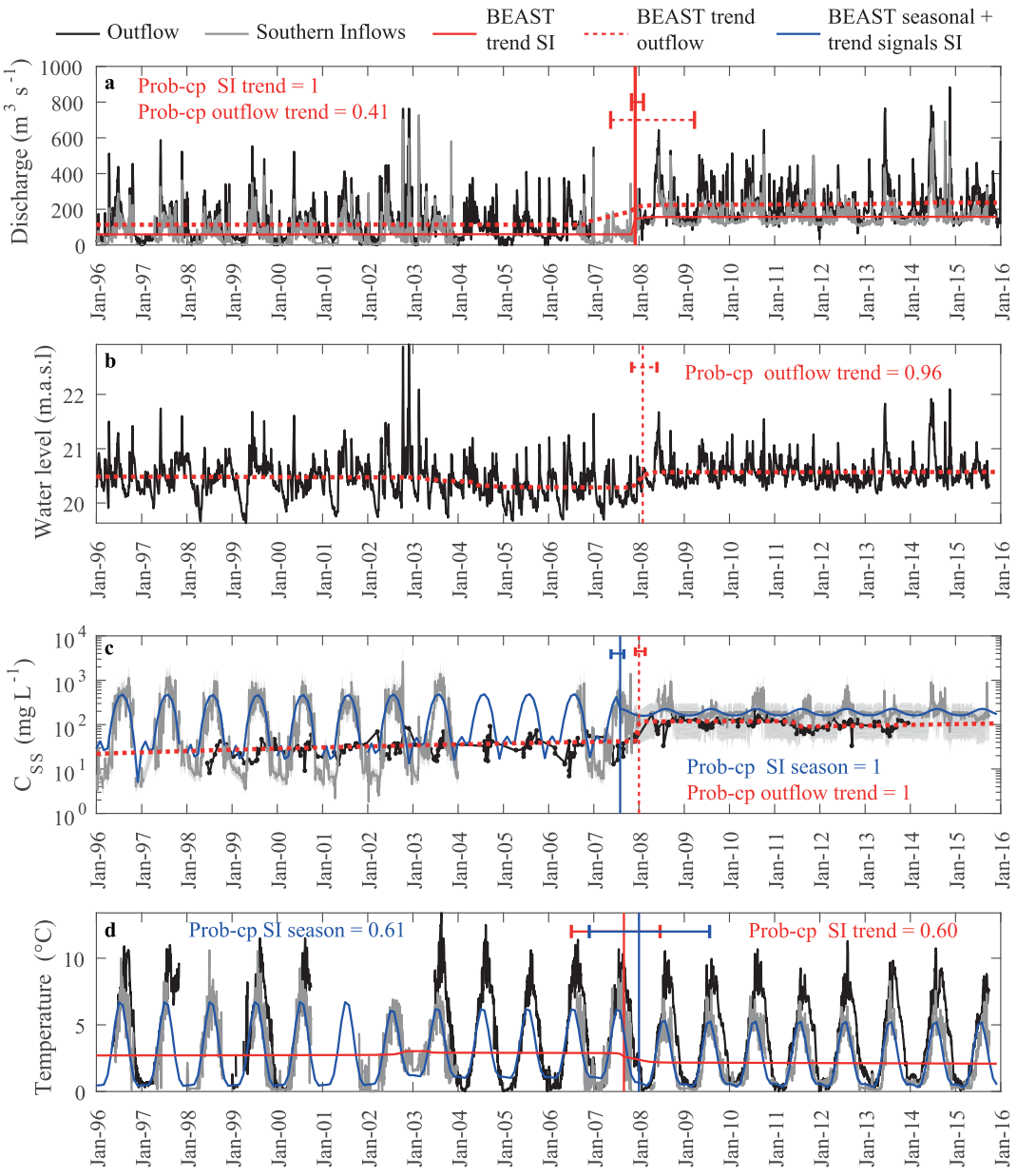

Fig. 2. Daily historical data on the Lake Lagarfljót southern inflow (SI) and outflow. (a) Discharge, (b) water level (meters above sea level) at the lake outflow, (c) suspended solid concentration, and (d) water temperature. The dots in (c) represent discrete measurements at the lake outflow (stations v7 and v325 in Fig. 1). The dark gray line in (c) shows the reconstructed time series for C_{SS} in the southern inflow using discrete samples collected in the JF river and the powerhouse, while the shaded grey area encompasses its uncertainty (details in section 4.3.1 in the main text). The BEAST algorithm was applied to monthly-averaged values. Vertical red and blue lines indicate the occurrence of a signal changepoint with occurrence probability (Prob-cp) > 0.3 in the trend and seasonal signals, respectively. The horizontal segments indicate their 95 % confidence interval. BEAST trends or seasonal + trend signals are displayed when changepoints are detected. (For interpretation of the references to colour in this figure legend, the reader is referred to the web version of this article.)

significantly; and (3) weather parameters governing atmosphere-water heat exchanges did not trend significantly during the same period. While linear trends are significant in the JF inflow temperature and discharge signals and in the southern inflow temperature signal, BEAST better describes (higher R^2) these underlying trend signals as abrupt changes occurring around 2008 (Fig. S2 e,f,h). This is especially the case for the southern inflow temperature where the probability of occurrence of a changepoint is close to one. This further suggests that changes in these variables are a direct effect of the Project.

Changes in the lake heat balance under summertime conditions also occurred as a result of the Project, as suggested by the significant cooling trends of the lake water surface temperature measured in mooring M1 (-0.166 °C $year^{-1}$) and the lake outflow (-0.084 °C $year^{-1}$, Table 1; Fig. S2). Cooling was also detected at the deepest thermistor in mooring M1, although this relationship was not statistically significant at 95 % confidence level.

4. Lake hydrodynamic modelling

4.1. Approach

The analysis of historical data has shown that the Project has led to significant changes in the lake hydrologic forcing, and, in background suspended-solid concentrations (Fig. 2, S2 and Table 1) resulting in decreased light penetration post-dam (Aðalsteinsson and Böðvarsdóttir, 2014). These changes can affect the lake internal dynamics, however

Table 1
Linear trends of mean summer (July to September) inflow, outflow and in-Lake variables at Lake Lagarfljót during the period 1995–2016. Bolded trends are statistically significant at ≥ 95 % confidence level.

Type	Location	Linear trend	R^2	p
Water Temperature	Southern inflows	**−0.083 °C yr^{-1}**	**0.623**	**0.047**
	- JF river	**+0.076 °C yr^{-1}**	**0.369**	**0.036**
	- Kelduá	−0.035 °C yr^{-1}	0.044	0.381
	Lake surface (M1, 1.5 m depth)	**−0.166 °C yr^{-1}**	**0.402**	**0.008**
	Lake deepwater (M1, 42 m depth)	−0.050 °C yr^{-1}	0.402	0.113
	Lake outflow	**−0.084 °C yr^{-1}**	**0.440**	**0.002**
Discharge	JF river	**−2.173 m^3/s yr^{-1}**	**0.409**	**0.006**
Weather	Air temperature	−0.004 °C yr^{-1}	0.000	0.944
	Wind speed	−0.009 m s^{-1} yr^{-1}	0.021	0.208
	Shortwave radiation	−0.798 W m^{-2} yr^{-1}	0.097	0.128

their specific contribution to alterations in the lake heat balance, the strength and duration of the density stratification, the dynamic of the river intrusion depths, and the amount of deep-water renewal remains to be assessed. Given the limited in-lake data available before the Project (only mooring M1 was present), the perturbations introduced by the project in the lake's internal physics must be analyzed through numerical modelling. While maintaining the same meteorological forcing, we propose a stepwise deconstruction from post-dam to pre-dam conditions, introducing a series of modifications in the hydrological forcing and initial conditions to simulate the pre-dam scenario (Fig. 3, summary Table S2). This procedure of deconstructing the post-dam scenarios towards pre-dam scenarios has advantages over directly running a hydrodynamic model with the pre-dam forcings: it allows isolating the effect of different hydrological processes altered by the Project itself and disassociates any possible effects of long-term changes in climatic forcing on the hydro-meteorological inputs.

4.2. Numerical model

Lake-hydrodynamics simulations were conducted using a parallel version (Acosta et al., 2010) of a three-dimensional primitive-equation (3D-PE) model that solves the layer-averaged form of the shallow water equations (Smith, 2006). Water density is a function of temperature and suspended sediment concentration, and it was assumed that particle settling was negligible during the simulation period, with no ice cover (see details and reasoning in Priet-Mahéo et al., 2019; Ramón et al., 2020). The momentum equations are solved on a staggered Cartesian grid, using a semi-implicit and three-level iterative leapfrog-trapezoidal finite difference scheme. Non-active- (i.e., tracers) and active-scalar (temperature and suspended solids) transport equations were solved using a two-level semi-implicit scheme, in which only vertical diffusion is discretized implicitly. Horizontal momentum advection is simulated using a first-order upwind algorithm. The advection terms in the transport equation for active and non-active scalars are discretized with a second-order flux-limiting scheme (e.g., Durran, 1999). Turbulent mixing is represented in the 3D-PE model using diffusion-like terms. A Laplacian operator with constant mixing coefficients K_h is used to represent the unresolved horizontal turbulent mixing of momentum and scalars. Vertical eddy coefficients of mixing K_z are calculated using the modified version of the Mellor and Yamada two-equation model (Mellor and Yamada, 1974) by Kantha and Clayson (1994). The present implementation of the model follows the formulation of Gross et al. (1999), which considers vertical diffusion as the only form of transport. The model was already validated for Lake Lagarfljót post dam (Priet-Mahéo et al., 2019).

4.3. Model setup for lake Lagarfjót

The computational domain extends from station v458 (Fig. 1) to the downstream end of the lake (Lagarfell, Fig. 1), and thus it comprised the full length of the lake plus a river reach of approximately 8 km upstream of the lake in its southern end. The domain was discretized with cells of 100 m in the horizontal direction ($\Delta x = \Delta y = 100$ m) and variable height in the vertical direction. Surface layer height Δz was set to 0.5 m and the successive layer heights were set to $\Delta z = (0.5 + 0.015n)$ m —being n the number of layers below the surface layer— until the maximum depth of the lake was reached. This amounts to a total of 93 layers, with a bottom layer height of 1.88 m. The time step was set to 60 s, the bottom drag coefficient C_d was set to 0.002 (Smith, 2006), and the Coriolis frequency f to 1.319×10^{-4} s^{-1} (65°N latitude). Horizontal viscosities and diffusivities were set to 0.5 m^2/s (Ramón et al., 2020).

The study period started on May 1st (day 121), around two months before stratification developed in the lake, and ended on October 23rd (day 296), around two weeks after the end of the stratification (see Priet-Mahéo et al., 2019). Simulations started using boundary condition data one month before (April 1st) the modeling period of interest (warm-up period). The lake was assumed initially at rest with uniform temperatures and C_{SS} matching those observed in the lake outflow in April at Lagarfell (Fig. 2 and Table S2).

The model was forced with the hourly-averaged atmospheric pressure, air temperature, relative humidity, and wind speeds and directions collected at meteorological station Met 1, and shortwave radiation collected at the meteorological station Met 2 during a rather typical year

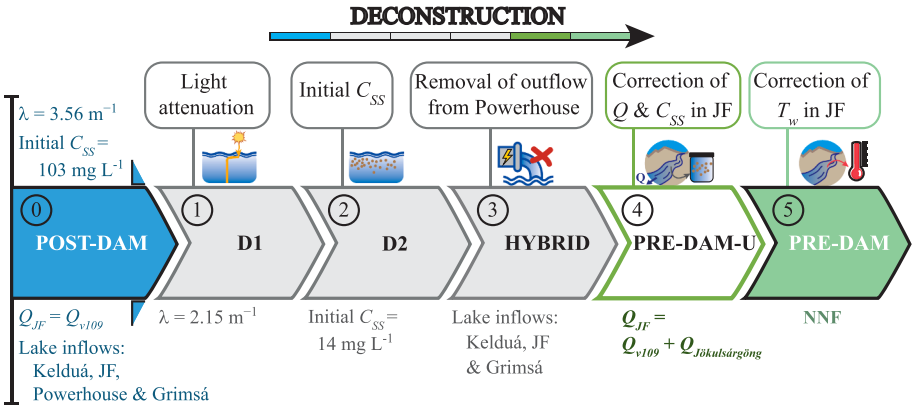

Fig. 3. Stepwise deconstruction from post-dam to pre-dam lake conditions. Each arrow contains the name in bold of each modeling ensemble scenario. Balloons on top of arrows in steps 1 to 5 indicate the main change introduced in the step. Specific changes in physical/hydrological variables introduced in steps 1 to 5 are indicated below each arrow.

2009 (Fig. S3 and see station locations in Fig. 1). Light attenuation coefficients λ were calculated based on observed maximum Secchi depth in the lake (Aðalsteinsson and Böðvarsdóttir, 2014), as in Martin and McCutcheon (1999), and were assumed to be constant throughout the simulation given the low variability within the scarce dataset.

The model incorporated daily river inflows collected at river Grimsá and the hourly temperature estimates for this river based on its correlation with temperatures in the Kelduá river as in Priet-Mahéo (2019) (Fig. S4a,b). Suspended-solid concentrations at Grimsá were assumed negligible based on available data on suspended solids for this river (Priet-Mahéo, 2019). At the downstream end, the model was forced with the hourly free surface elevation collected by the Icelandic Meteorological Office (IMO) at Lagarfell post dam. Upstream, the model was forced with hourly data on river discharge, temperature, and C_{SS} for the southern inflow, which varied in the different modeling scenarios.

4.3.1. Post-dam scenario

Our starting point, step 0, is the post-dam scenario (Fig. 3, more details in Table S2), in which lake hydrodynamics post-dam is forced with hydrological (Fig. 4, details in Fig. S4) and meteorological (Fig. S3) data collected in 2009. The scalar (temperature and C_{SS}) time signals for the southern inflow were constructed as in Priet-Mahéo et al. (2019) and Ramón et al. (2020), assuming that the outflows from the powerhouse, and the Kelduá and JF rivers completely mixed before entering the lake. River temperatures were continuously measured by IMO and Landsvirkjun at various gauging stations (Fig. 1), enabling a straightforward calculation of the volumetric weighted average water temperature of the three confluent streams (Fig. 4b). However, only sparse discrete samples of suspended solid concentrations (C_{SS}) were available for the different inflows to the lake. Therefore, the times series of C_{SS} on each tributary needed to be first reconstructed.

C_{SS} at Kelduá river were assumed negligible (=0 kg m^{-3}) based on available data on suspended solids for this river by IMO (see also Priet-Mahéo, 2019). C_{SS} in the glacial JF river were estimated from two different rating curves depending on the time of the year (details on how we obtain these rating curves and statistics in Text S2 in supporting information):

$$log_{10}(F_{SS-JF}) = (2.301 \pm 0.192) \times log_{10}(Q_{JF}) - (2.668 \pm 0.320) \quad (1a)$$

$$log_{10}(F_{SS-JF}) = (1.682 \pm 0.251) \times log_{10}(Q_{JF}) - (2.304 \pm 0.261) \quad (1b)$$

where F_{SS} and Q are the suspended-solid mass flux (kg s^{-1}) and river discharge (m^3 s^{-1}), respectively. Eq. (1a) and Eq. (1b) represent the best fits (and the 25–75 percentile uncertainty calculated with the boostrap method) for the periods covering mid-May until the end of October (R^2 = 0.849), and the rest of the days of the year (R^2 = 0.664). C_{SS} at the powerhouse showed poor correlation with flow rates (Priet-Mahéo et al., 2019). The uncertainty in C_{SS} both in the JF river (wide confidence intervals in the rating curves) and in the powerhouse outlet (sparse data and poor correlation with discharges) translate into uncertainties in the calculations of water density of the southern inflow.

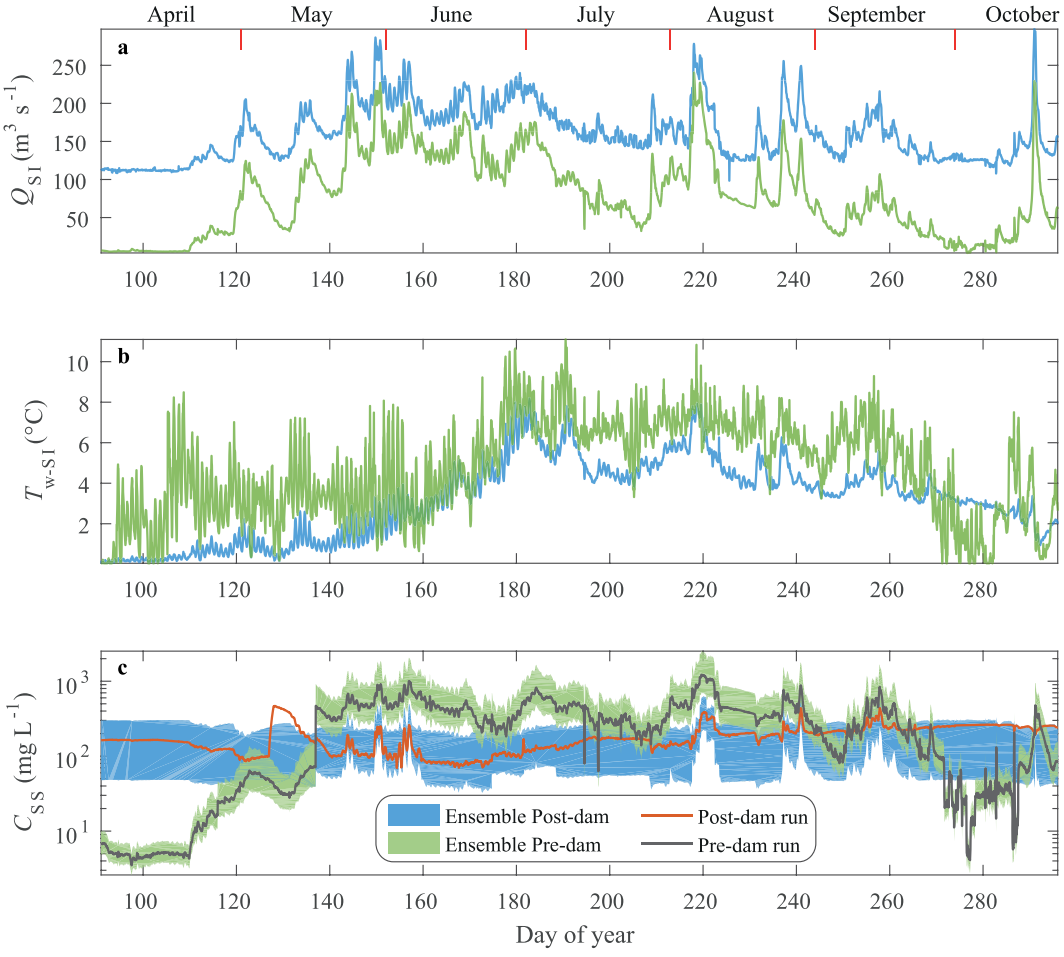

Fig. 4. Hourly hydrological forcing for the southern inflow in the Post-dam (step 0) and Pre-dam (step 5) ensembles and runs. (a) Southern inflow discharges, (b) inflow temperature, and (c) suspended-solid concentration (reconstructed from measured discrete samples). The blue and green areas in (c) show the range of variability of C_{SS} in the Post-dam and Pre-dam ensemble runs. (For interpretation of the references to colour in this figure legend, the reader is referred to the web version of this article.)

To account for uncertainty in the C_{SS} content of the southern inflow, two types of simulations were conducted in the post-dam scenario. First, in our reference Post-dam run, we used the best-fit coefficients in Eqs. (1a),b to estimate the time-varying C_{SS} in the JF river (Fig. S4c). C_{SS} at the powerhouse outlet were linearly interpolated from ≈ monthly observations collected in 2009 (Fig. S4c). The resulting volumetric weighted average C_{SS} signal for the southern inflow in the reference Post-dam run is represented by a black line in Fig. 4c. A second exercise consisted of conducting an ensemble of simulations (hereon Post-dam ensemble) forced with southern inflows carrying different suspended sediment loads (see final uncertainty ranges of C_{SS} in blue in Fig. 4c). The time series of suspended concentrations in each simulation of the ensemble was constructed with independent and random realizations of 5 parameters: the two intercepts and slopes of the logarithmic JF rating curves and C_{SS} in the powerhouse outlet (assumed to be constant through time in each simulation). The range of plausible values for the intercepts and slopes of the JF rating curves covers the 25 and 75 percentiles determined using the bootstrap method (Eqs (1a,b) and blue and grey shaded areas in Fig. S5). The range of plausible values for C_{SS} in the powerhouse outlet post-dam (recall that $C_{SS} = 0$ pre-dam) was determined by fitting a Generalized extreme value (GEV) distribution to the measured values (Fig S6). C_{SS} were allowed to vary within the maximum probability range $\mu \pm \sigma$; μ and σ being the location parameter and the scale parameter in GEV (Fig. S6). The parameter space was sampled using a Latin Hypercube Sampling (LHS) technique (McKay et al., 1979) from independent uniform distributions spanning the established ranges for each parameter. The LHS comprises 1000 samples per parameter. Note however that, due to the high computational cost of the simulations, we only used 40 of these random combinations.

4.3.2. Deconstructed scenarios

The post-dam scenario was deconstructed in a stepwise manner to evaluate step-by-step the added effect of the different changes introduced by the Project in the hydrological forcing and the lake background conditions (Fig. 3, Table S2). In step 1 (scenario D1), light attenuation was lowered to match measured values pre-dam (Aðalsteinsson and Böðvarsdóttir, 2014). In step 2 (scenario D2) the initial background turbidity in the lake water column was adjusted to pre-dam April conditions. In step 3 (Hybrid scenario) the outflow from the powerhouse was removed. In step 4 (Pre-dam-U scenario) discharges in the JF river were increased to pre-dam conditions by returning to this river the fraction that was diverted to the power plant from the Ufsarlón pond through the Jökulsárgöng intake (Fig. 1, Fig. S4d). C_{SS} in the JF river were adjusted accordingly. Finally, in step 5 (Pre-dam scenario) water temperature in the JF river was also adjusted to account for the effect of increased river discharges pre-dam on river temperatures. Discharges in the Kelduá river were not modified in any of the deconstructed scenarios given the small entity of the diversions from the Kelduárlon reservoir to the Ufsarlón pond (Landsvirkjun's communication).

In steps 4–5, higher discharges in the JF river pre-dam affected two variables: C_{SS} (step 4) and water temperature (step 5). An ANOVA test (details in Text S2) comparing suspended-solid rating curves post- and pre-dam indicated that rating curves in the JF have not been significantly altered post-dam. Thus, the same rating curves to calculate C_{SS} in the JF river (Eqs. (1a-b)) were used for pre-dam and post-dam conditions, and differences in C_{SS} are only the result of modifications in JF discharges (Fig. S4 d,e). Significant warming in the JF river during summer (Table 1 and Fig. S2e) matching no significant trends in the air temperature and solar radiation (Table 1, Fig. S2), suggests that the increased JF water temperatures are largely driven by the lower discharges in the JF river post dam (Fig. S2f). To estimate JF water temperature prior to damming, we applied a Neural Network Fitting (NNF) Approach. The shallow neural network had 100 neurons and was optimized with the Levenberg-Marquardt algorithm. The reference period for the fitting expands seven years after damming, from August 2008 to September 2015, when data on solar radiation was available at Met 2. 70 % of the reference data was used to train the neural network, 15 % for validation, and the remaining 15 % for testing. Analysis was restricted to the period covering April to November when temperature loggers in JF recorded temperatures above 0 °C. Hourly meteorological variables (air temperature, shortwave radiation, air pressure, RH, wind velocity), JF discharges and river Kelduá temperatures were used as inputs to the network. The performance of the network was satisfactory, with $R^2 = 0.89$ and a root mean square error of 1.04 °C (Fig. S7). JF temperatures in the Pre-dam scenario (step 5) were calculated with the network, using the modified discharges in the JF river (Fig. S4 d,f).

As for the post-dam scenario (Section 4.4.1), each deconstructed scenario (steps 1 to 5 in Fig. 3) is composed of an ensemble of 40 simulations that account for the uncertainty in suspended-solid concentrations in the JF river (steps 1 to 5) and the powerhouse (steps 1 and 2). In step 5, we will refer to the simulation where the contribution of C_{SS} in the JF river to the volumetric weighted average C_{SS} in the southern inflow ($=C_{SS\text{-}JF} \times Q_{JF} \times Q_{SI}^{-1}$) was calculated with the best fit coefficients in Eqs.1a,b as the reference Pre-dam run. Discharge, and the volumetric weighted average water temperature and C_{SS} in the southern inflow for the Pre-dam ensemble and reference Pre-dam run are shown in Fig. 4.

4.4. Lake thermal balance

The contribution of the atmospheric and advective heat fluxes through river inflows to the variation of the lake's average temperature on a given day n, ΔT_{aver_n}, was calculated as (e.g., Posada-Bedoya et al., 2021):

$$\Delta T_{aver_n} = (T_{aver_n} - T_{aver_{n-1}}) = \underbrace{\Delta t \frac{S_{total_{n-1}} Q_{Heat-Atm_{n-1}}}{\rho_{n-1} c_p V_{total_{n-1}}}}_{\Delta T_{Atm}} + \underbrace{\Delta t \frac{Q_{SI_{n-1}}}{V_{total_{n-1}}} (T_{SI_{n-1}} - T_{aver_{n-1}})}_{\Delta T_{SI}} + \underbrace{\Delta t \frac{Q_{\acute{G}rimsa_{n-1}}}{V_{total_{n-1}}} \left(T_{\acute{G}rimsa_{n-1}} - T_{aver_{n-1}}\right)}_{\Delta T_{\acute{G}rimsa}} - \underbrace{\Delta t \frac{Q_{Out_{n-1}}}{V_{total_{n-1}}} (T_{out_{n-1}} - T_{aver_{n-1}})}_{\Delta T_{Out}} \quad (2)$$

Here T_{aver_n} is the modeled lake's average temperature on day n. The first term of the right-hand side ΔT_{Atm} represents the contribution of the heat exchanges with the atmosphere and the second to fourth terms account for the advective exchanges ΔT_{Adv} through the southern inflows ΔT_{SI}, river Grimsá $\Delta T_{Grimsá}$ and the lake outflow, ΔT_{Out}. S_{total} and V_{total} are the lake surface area and lake volume, respectively; ρ is water density; T_{SI}, T_{Grimsa}, and T_{out} are the inflow and outflow water temperatures; c_p the specific heat of water; Δt is the time interval (=1 day), and $Q_{Heat\text{-}Atm}$ is the lake-averaged net surface heat flux resulting from lake exchanges with the atmosphere and calculated as:

$$Q_{Heat-Atm}(t) = \frac{1}{S_{Total}} \sum \begin{bmatrix} Q_{SWR}(t) + Q_{LWR}(t,x,y) + Q_S(t,x,y) \\ +Q_L(t,x,y) \end{bmatrix} \Delta x \Delta y \quad (3)$$

where Q_{SWR} (t) and Q_{LWR} (t,x,y) are the net short-wave and long-wave radiation heat fluxes, and $Q_S(t,x,y)$ and $Q_L(t,x,y)$ are the sensible and latent heat fluxes for each grid cell at the free surface. These latter two terms are calculated using bulk aerodynamic coefficients (Kondo, 1975). A negative sign in the heat fluxes represents lake heat loss. Our analysis

will focus on the impacts of the Project on ΔT_{SI} and its relative contribution to changes in ΔT_{aver}. The analysis will be conducted on a monthly basis.

4.5. Lake water stability, stratification, river intrusion depth, and tracer experiments.

The resistance of the water column to mechanical mixing, and thus the strength of stratification, was assessed with the Schmidt stability (Idso, 1973):

$$St = \frac{g}{A_s}\int_0^H (z - z_v)\rho_z A_z dz \quad (4)$$

Where g is the gravity acceleration, A_s is the lake surface area, A_z and ρ_z are the lake area and water density at depth z, and $z_v = \int_0^H zA_z dz / \int_0^H z dz$ is the depth to the center of volume of the lake. A threshold value of 100 J m^{-2} in the stability of the water column was also used to define the start and end of the stratification period (e.g., Engelhardt and Kirillin, 2014; Yankova et al., 2016). The epilimnion in the density profiles was identified following Priet-Mahéo et al. (2019), as the layer where densities differ at most 0.03 kg m^{-3} from the surface density. Similarly, the hypolimnion was taken as the layer where densities differ at most 0.03 kg m^{-3} from bottom densities. The depth of the pycnocline h was taken midway between the bottom of the epilimnion and the top of the hypolimnion.

Ramón et al. (2020) showed that the gradient Richardson number Ri_ρ (Wells and Wettlaufer, 2007) was a good predictor for the intrusion behavior of the southern-inflow river plume. It is defined as

$$Ri_\rho = g'_{12}\frac{h}{B_0^{2/3}} \quad (5)$$

Here ρ_0, ρ_1 and ρ_2 are the southern-inflow density and surface and hypolimnetic lake densities, $g'_{12} = g(\rho_2 - \rho_1)/\rho_1$ is the reduced gravity of the ambient water density step and B_0 is the inflow buoyancy flux per unit width of the gravity current. The buoyancy flux, in turn, is calculated as $g'_0 Q_0/W$, from the inflow reduced gravity $g'_0 = g(\rho_0 - \rho_1)/\rho_1$, the river flow rate Q_0 and the river width W. If $Ri_\rho < 0$ the inflow river has a lower density than the lake surface ($\rho_0 < \rho_1$) and the river plume will remain near the surface, forming overflows. If $Ri_\rho > 0$, the river plume is negatively buoyant. It will intrude as an interflow if Ri_ρ exceeds a critical value Ri_ρ* or $\rho_0 < \rho_2$; otherwise, it will penetrate through the ambient-water density step forming underflows. The critical Ri_ρ* was estimated from the slope-dependent parameterization proposed by Wells and Wettlaufer (2007), using the average longitudinal slope θ of 1.8° observed in Lake Lagarfljót, as $Ri_\rho^* \approx 26.9304(\sin\theta)^{1/3} \approx 8.5$. We will use Ri_ρ to analyze the behavior of the river plume during the thermal stratification period in the different modeling scenarios.

To quantify how effectively deep water is renewed during the stratification period, lake water below 70 m was numerically traced with a tracer of 100 ppm concentration at the onset of the thermal stratification, when the isopycnals were nearly horizontal. The mass of tracer below 70 m was tracked for all ensemble runs.

5. Results

5.1. Lake thermal balance: the importance of advective heat fluxes from the southern inflow

The lake warms from May to August (net positive ΔT in Fig. 5) and cools thereafter. After the Project, heating is primarily controlled by the heat exchange with the atmosphere until July-August when heat advected by the southern inflows becomes comparable in magnitude (Fig. 5). The southern inflow acts almost continuously as a cooling source for the lake post-dam, which as explained in section 3, is related

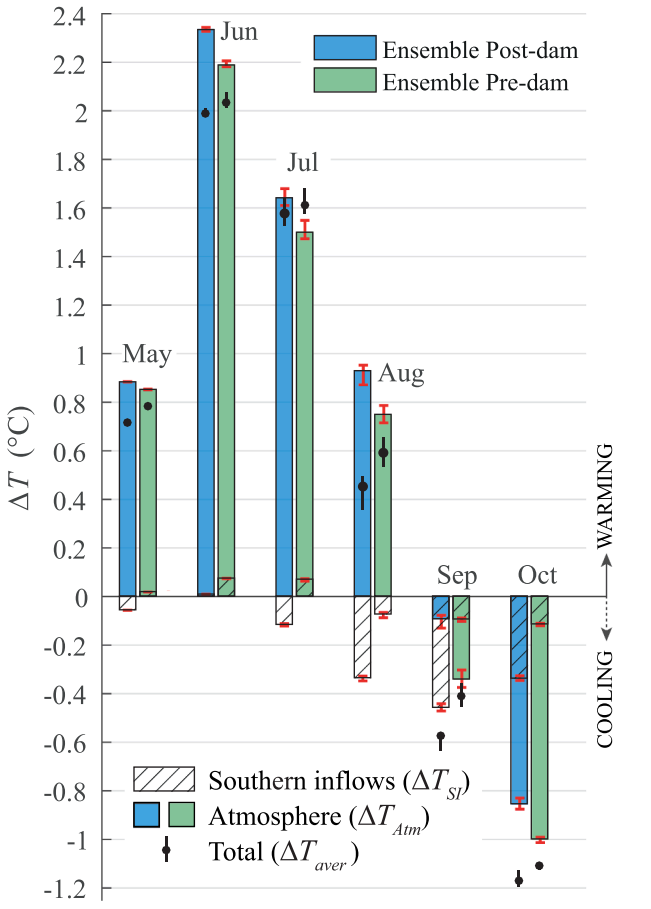

Fig. 5. Impact of the Project on the lake thermal balance. Modeled net monthly contribution to the change of the average lake temperature ΔT_{aver} by the surface heat exchanges with the atmosphere ΔT_{Atm} and by the advective fluxes by the southern inflow ΔT_{SI} (Eq. (2)). The bars and dots show mean values per ensemble and the whiskers the 95-confidence-interval.

to the creation of the deep Hálslón reservoir, the deep intake of the reservoir, and the subterranean transport to the powerhouse. All three factors limit the atmospheric heat exchange, aka warming potential, of the glacial water. The contribution of the southern-inflow to the change in the lake's mean temperature represents ≈36 % and ≈38 % of the contribution of atmospheric exchanges in August and October, respectively, and exceeds it (by ≈500 %) in September. This is in sharp contrast to the pre-dam scenario in which the monthly contribution of the southern inflow to the changes in the lake's mean temperature represented only ≈10 %, ≈ 28 % and ≈11 % of the contribution via atmospheric exchanges in August, September and October, respectively. Moreover, pre-dam southern inflows acted as a warming source for the lake from May to July.

5.2. Length of the stratification period and stability of the water column

The modeled water column stability at the deepest point of the lake is presented in Fig. 6. The period of thermal stratification shortened as a result the Project, starting (Schmidt stability > 100 J m^{-2} in Fig. 6a) 6 days later (median values on days 185 and 179, respectively), and ending 9 days earlier (median value on day 275 and 284) post- vs. pre-dam. When suspended solids are also taken into account (Fig. 6b), the onset of density stratification pre-dam occurs one month earlier (day 151; see the green shadowed area in Fig. 6b), while remaining unchanged post-dam (day 185). This suggests that the total length of density stratification decreased from ≈ 4.5 months to ≈ 3 months after the Project. The earlier onset of density stratification in the lake pre-dam

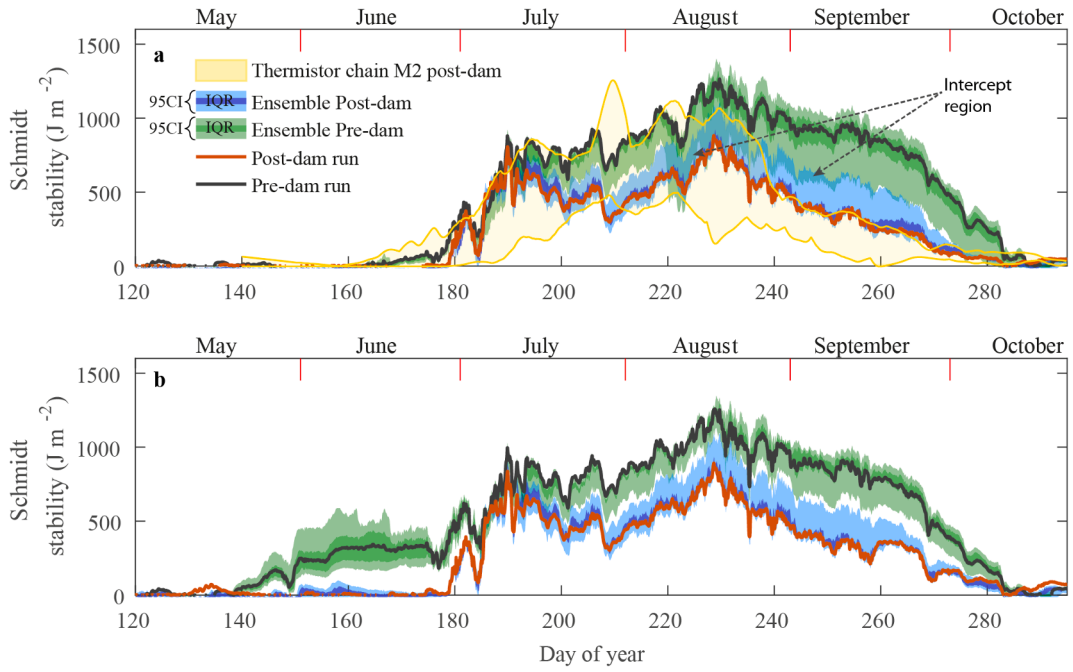

Fig. 6. Post-dam vs. pre-dam water column stability. Time series of Schmidt stability of the water column at the deepest point, location M2 in Fig. 1a, calculated from the modeled (a) thermal and (b) density (temperature and suspended solids) stratification. The shaded transparent blue and green areas represent the 95 confidence interval for the ensemble runs. Shaded darker blue and green areas show the interquartile range (IQR) for the Post-dam and Pre-dam ensembles, respectively. The shaded transparent yellow area in (a) displays the range of values of thermal stability calculated from the thermistor chain M2 from 2009 to 2013. (For interpretation of the references to colour in this figure legend, the reader is referred to the web version of this article.)

is only observed in the Pre-dam-U (step 4) and Pre-dam (step 5) ensembles (see Fig. S8), which suggests that those changes are likely caused by the seasonal sediment load variation in the undammed JF.

The strength of the stratification was also higher pre-dam. For example, stability reaches values up to 900 J m^{-2} and 1300 J m^{-2} at the time of maximum stratification in the Post-dam and Pre-dam reference runs, respectively (red and black lines in Fig. 6b). The wide range of stabilities existing in the simulation ensembles points to a strong dependence of lake water stability on the sediment concentration in the southern inflows. However, the interquartile ranges of the Pre-dam and Post-dam ensemble stabilities series (dark blue and dark green shadow areas in Fig. 6a,b) narrow around the stability values of the two reference runs, and the 95 % confidence bands (light blue and light green shadow areas in Fig. 6a,b) hardly overlap, indicating that the changes introduced by the Project in water column stability have been significant (statistically). Not accounting for temperature corrections of the JF river—step 4, ensemble Pre-dam-U— would introduce an offset towards even higher stabilities pre-dam (Fig. S8). This effect is however lower than that associated with the uncertainty on C_{SS}.

The water-column stabilities of the Pre-dam ensemble lie outside the range of stability values calculated with thermal observations with mooring M1 post-dam (green vs. yellow shaded areas, Fig. 6a) during the second half of the stratification period. This provides further support that the lower stability values observed post-dam are indeed a direct impact of the Project itself, and higher values of thermal stability, such as those in the Pre-dam ensemble, can no longer be achieved due to the different combinations of meteorological and hydrological forcing occurring in the lake post-dam. The occurrence of lower lake stability values post-dam is additionally supported by stability values calculated from the thermistor chain M1 deployed from 2000 to 2015 at a shallower location. A statistically significant changepoint in its seasonality was detected at the end of 2007, coinciding with the time when the power plant became operational (Fig. S9).

Monthly average density profiles demonstrate that pre-dam a metalimnion developed within the top 50 m of the water column, while post

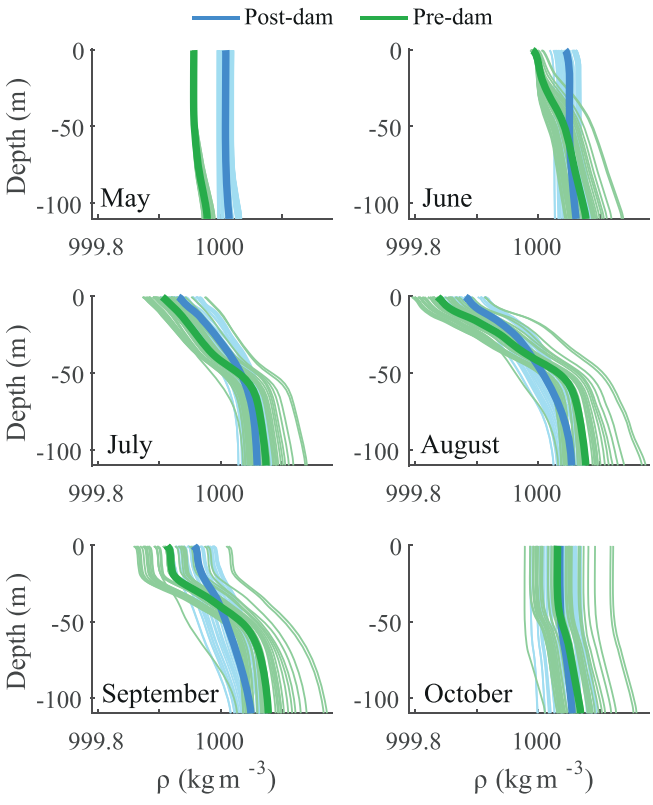

Fig. 7. Post-dam vs. pre-dam water column density profiles. Modeled monthly-averaged water density at the deepest point, location M2 in Fig. 1a, in the Post-dam and Pre-dam ensemble runs. Thick blue and green lines show average values per ensemble. (For interpretation of the references to colour in this figure legend, the reader is referred to the web version of this article.)

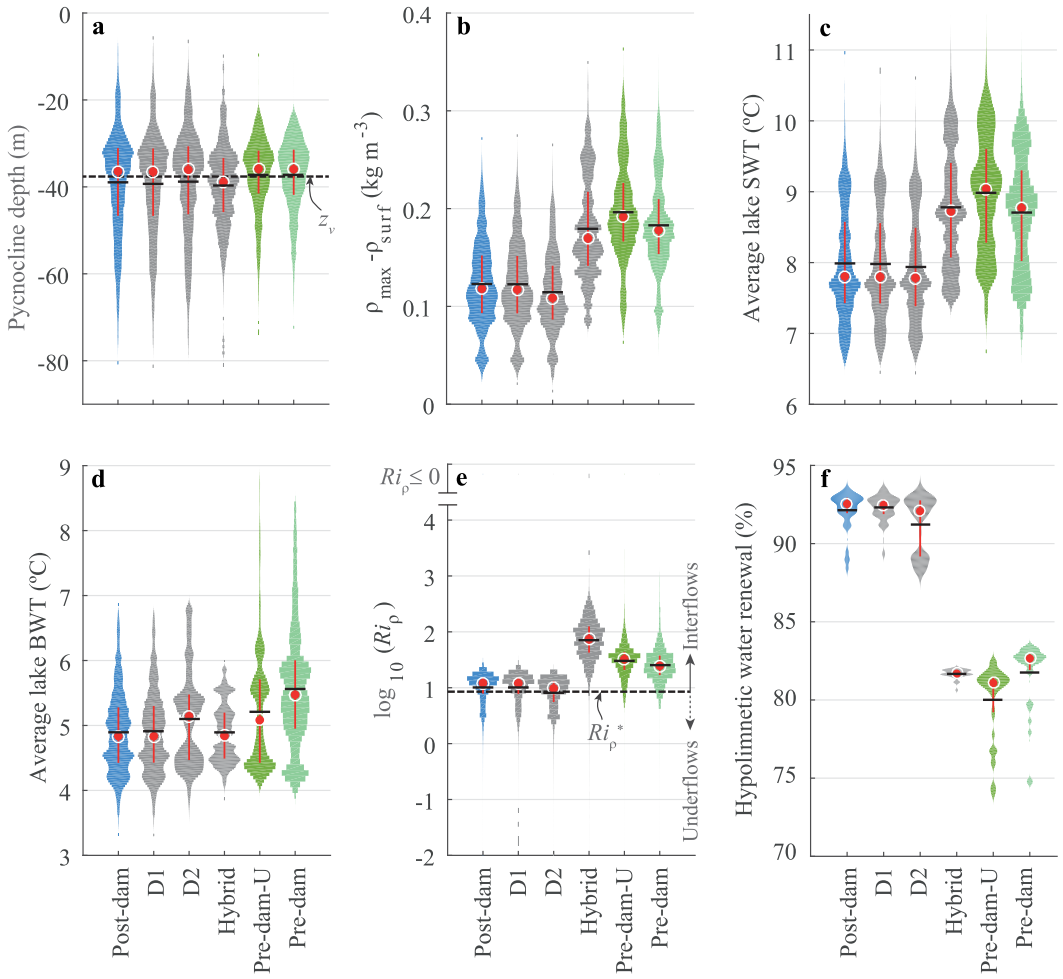

Fig. 8. Impact of the Project on the characteristics of the thermal stratification period in Lake Lagarfljot. Violin histograms per ensemble scenario showing the range of variability of (a) the depth of the pycnocline, (b) top–bottom lake density differences, (c-d) lake-averaged surface water temperature SWT and bottom (100-m-deep) water temperature BWT, and (e) gradient Richardson number within the thermal stratification period in the lake, and (f) the percentage of hypolimnetic water that is renewed. Red dots and vertical error bars show the median and interquartile range per ensemble. Solid black horizontal lines show mean values per ensemble. The horizontal dotted line in (a) and (e) indicates the depth of the center of volume of the lake, z_v, and $Ri_\rho^* = 8.5$. (For interpretation of the references to colour in this figure legend, the reader is referred to the web version of this article.)

dam, the entire water body was linearly stratified (Fig. 7). The pycnocline position remains, however, close to the center of gravity of the lake ($z_v \approx 38$ m on average) in all modeled scenarios (Fig. 7 and 8a). The higher water column stability pre-dam is mainly due to larger top–bottom density differences in the water column, which, on average, double those modeled post-dam (Fig. 8b). The new inputs from the powerhouse resulted in a median cooling of ≈1°C and 0.6 °C in the modeled surface and deep (100 m) layers of the lake (Figs. 8c-d) during the thermal stratification period. The maximum stability differences between the Pre-dam and Post-dam ensembles occur during the second half of the stratification period, coinciding with the period of the highest relative contribution of the southern inflows to the heat balance of the lake (see Fig. 5). For example, the reference Post-dam and Pre-dam runs reach a maximum difference of ≈ 600 J m^{-2} in September (Fig. 6b).

5.3. River intrusion depths and deep-water renewal during the thermal stratification period

The changes introduced by the Project in the southern inflows also modified the inertial-buoyancy equilibrium and, as a result, the inflow dynamics. In both the pre- and post-dam periods, the southern-inflow river plume tends to form metalimnetic intrusions under stratified conditions. However, the probability of southern inflows leading to underflows has increased post-dam, as indicated by the occurrence of values of $Ri_\rho < Ri_\rho^*$ being 27 % (Fig. 8e), compared to ≈5% pre-dam.

As demonstrated by Ramón et al. (2020), wind-driven large-amplitude isopycnals displacements, reaching up to 70 m, along with the occurrence of successive underflows, effectively contribute to deep-water renewal in the lake post-dam. Indeed, in the Post-dam ensemble, a significant portion of the tracer mass (92.5 % on average) injected at depths deeper than 70 m was renewed by the end of the thermal stratification period (Fig. 8f). The ensemble scenarios reveal that removing the new input from the powerhouse resulted in a reduced probability of underflows (Fig. 8e) and an increase in water column stability (Fig. 6 and S8) during the pre-dam thermal stratification period. Consequently, the percentage of deep-water renewal at the end of the stratification period decreased to an average of 80 % in the Pre-dam ensemble (Fig. 8f), despite a longer stratification period in this case. The average rate of deep-water renewal in the Pre-dam ensemble was ≈ 80 % of the average rate modeled in the Post-dam ensemble. A schematic summarizing the primary impacts of the Project is presented in Fig. 9.

6. Discussion

This study demonstrates a significant reduction in water column stability in Lake Lagarfljót resulting from a series of changes introduced

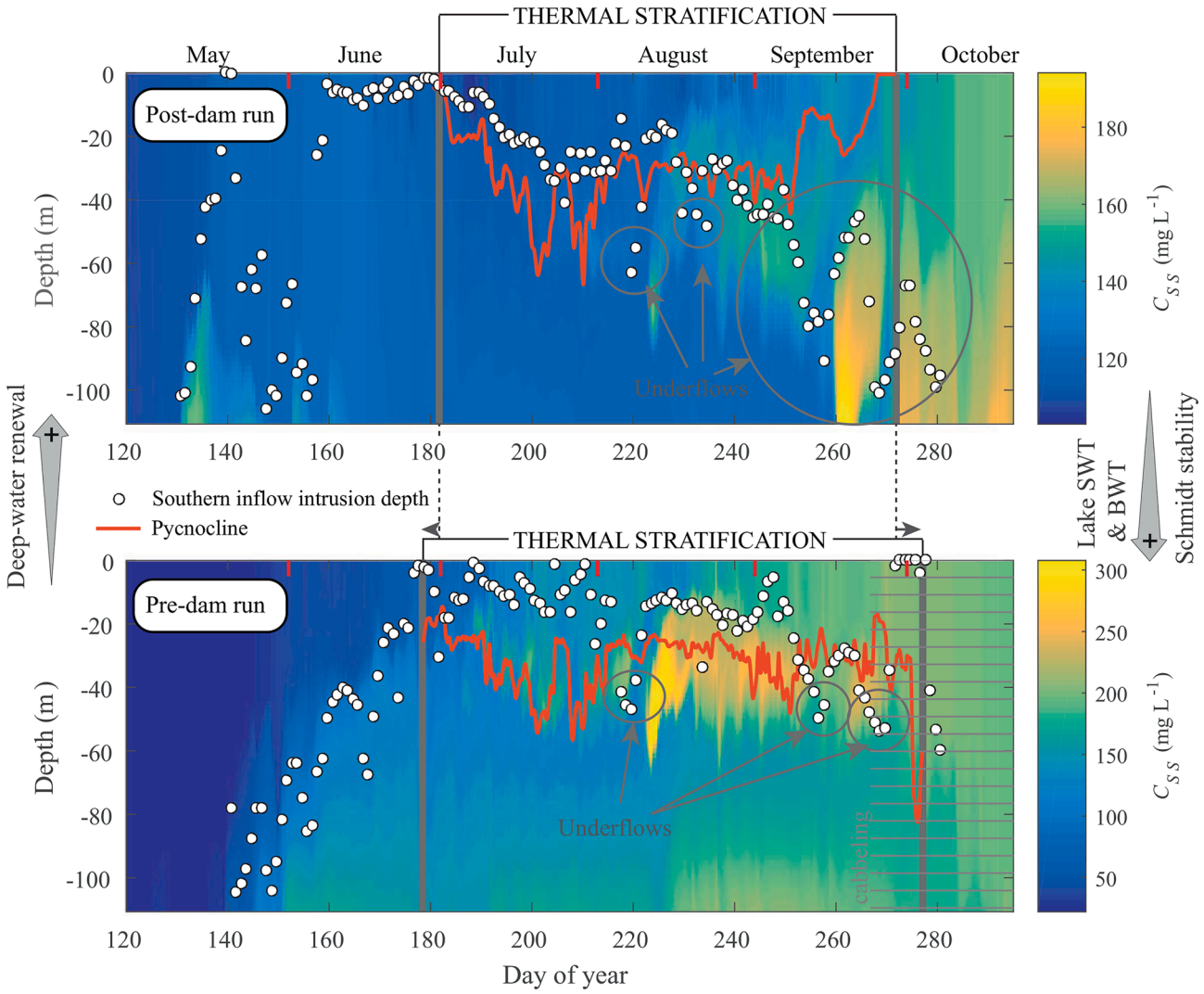

Fig. 9. Schematic summarizing the primary impacts of the Kárahnjúkar hydroelectric project, illustrating water pathways (southern inflow intrusion depths depicted as white circles) and sediment pathways (modeled C_{SS} at the deepest location of the lake; location M2) from May to October in Lake Lagarljót. Post-dam, a decrease in lake surface water temperature (SWT), bottom water temperature (BWT) and C_{SS} was observed, along with the lengthening of the thermal stratification period and a decrease in its strength due to the project. Additionally, underflows (southern-inflow intrusion depths below the pycnocline), became more frequent during the thermal stratification in the post-dam period, contributing to increased deep water renewal in the lake. Southern inflow intrusion depths were estimated by introducing pulses of a numerical tracer into the southern inflow as in Ramón et al. (2020).

by the Kárahnjúkar Hydroelectric Project in the lake's hydrological forcing. Our stepwise approach allowed us to identify that the changes in stability are primarily attributed to increased inflows from and the cooling effect of deep-water diversions from the Hálslón reservoir (step 3, Fig. 6 and S8). The effects of changes in light attenuation or the initial background suspended solid concentration C_{SS} in the lake (steps 1 and 2) are comparatively minor. Lake Lagarfljót already had high light attenuation in the pre-dam period ($\lambda = 2.7$ m^{-1}), and C_{SS} in the southern inflow exceeded the initial background lake concentration as early as April. Adjusting discharges, C_{SS}, and water temperature in the natural glacier tributary to the lake — the JF river— to pre-dam conditions (steps 4 and 5) moderates the impact of removing water diversions from Hálslón reservoir. However, a difference of O(1 0^{2}) J m^{-2} is still detected at the deepest location between post-(step 0) and pre-dam (step 5) conditions. The stepwise approach allowed us to assess the cumulative effect of the evaluated alterations and to identify which added element impacted the summer stratification in the lake the most.

The shape of the lake density profiles also exhibited differences in the pre-dam period. Priet-Mahéo et al. (2019) demonstrated that strong wind-driven shear at the base of the surface mixed-layer and the upwelling of deep metalimnetic layers resulted in a nearly continuous density stratification in the shallowest 70 m after the dam was constructed (Fig. 7). However, during the pre-dam period, the river plume acted almost continuously as a source of metalimnetic water (Fig. 9) during the thermal stratification period, contributing to the formation of a distinguishable metalimnion (Fig. 7). The reduced stability of the water column and the presence of deep intrusions during the thermal stratification period (Figs. 8e and 9) favor the nearly complete water renewal of the hypolimnetic water post-dam. In contrast, the pre-dam deepwater renewal, while still significant, decreased to approximately 80 % (Fig. 8f). The significance of underflows in the deep-water renewal of Lake Lagarfljót was highlighted by Ramón et al. (2020), although it becomes even more critical in the deep-water renewal and water quality of temperate lakes (e.g., Fink et al., 2016). For instance, declines in oxygen levels in the deep waters have been linked to increases in the strength of thermal stratification in these lakes (Ito and Momii, 2015; Jane et al., 2021).

While Ri_{ρ} proves to be a reliable predictor for the intrusion behavior of the southern-inflow river plume Ramón et al., (2020), there is also evidence of cabbeling, which is the formation of mixed water parcels

that are denser than the mixing source fluids due to the non-linearity of the equation of state with temperature, affecting the southern-inflow intrusion dynamics (examples in Fig. S10 and S11). For cabbeling to influence deep-water renewal beyond what Ri_p captures, the mixing of the southern inflow and the lake epilimnetic water—both with a lower density than the hypolimnetic water—should yield mixed water parcels denser than the hypolimnetic water in the lake. This condition is met for ≈ 2 % of the simulated period in the Post-dam reference run; however, it rises to ≈ 11 % in the Pre-dam reference run (Fig. S12). In the pre-dam period, cabbeling was recurrent at the end of the stratification period (day > 266, Fig. 9), influencing the "autumn" mixing overturn, similar to observations by Carmack et al. (1979) in 50°N Kamloops Lake.

Convective sedimentation and lofting could also be at play in both the pre-dam and post-dam periods. The southern inflow river plume lies in the lofting and convective regime diagram presented by Lu et al. (2022) (Fig. S13). However, our simulations did not account for particle settling. Priet-Mahéo et al. (2019) demonstrated that their model results accurately reproduced the evolution of the C_{SS} signal measured at the lake outflow in 2009 despite assuming no settling of particles. They also showed good agreement between modeled and measured (moorings) temperature data at three locations in the lake for the same year. The assumption of negligible deposition aligns with the finding of Striberger et al. (2011) that most of the sediments or rock flour brought by the JF river stay in suspension in the water during the summer and deposits during the winter. However, our model results overpredicted C_{SS} in the lake outflow in the pre-dam period by almost threefold (Fig. S14), suggesting that the assumption of negligible particle settling may not hold in this period. Accounting for particle settling in the Post-dam and Pre-dam reference runs did not modify the detected main impacts of the Project on the lake thermal dynamics (Fig. S15).

Air-water heat exchange continues to dominate the seasonal heat balance in the subarctic Lake Lagarfljót. This finding aligns with the analysis by Posada-Bedoya et al. (2021). They demonstrate that in low residence-time lakes, the contribution of heat advection can only dominate the seasonal heat budget in tropical and subtropical systems where the seasonal amplitude of heating–cooling rates resulting from air-water heat exchange is lower compared to medium and high-latitude lakes. Still, we found that post-dam advective heat fluxes have become comparable in magnitude $|\Delta T_{Adv}/\Delta T_{Atm}| \sim 1$, or even dominate, $|\Delta T_{Adv}/\Delta T_{Atm}| > 1$, the lake heat balance during the second half of the thermal stratification period (August to October, Fig. 5). The net effect of the southern inflows is to cool the lake throughout most of the study period. This cooling trend during the thermal stratification period due to advective processes is consistent with findings from other low residence-time lakes (≲ 4 yr) in temperate regions (Carmack et al., 1979; Råman Vinnå et al., 2018; Valerio et al., 2015). From May to October, total advective heat exchanges account for a ≈ 2 °C and ≈ 0.5 °C cooling of the lake in the Post-dam and Pre-dam ensembles, respectively (Fig. 5). The results from these ensembles indicate that the new inputs from the powerhouse lead to cooling of both the surface (median ≈1°C, Fig. 8c) and deep (median ≈0.6 °C, Fig. 8d) layers of the lake during the thermal stratification period. These findings are consistent with the measured temperature values at M1 and M2 locations (Fig. S2 and S16).

Not only has the stability decreased and the water cooled as a result of the Project, but there have also been significant changes in the lake's phenology. The onset of thermal stratification now occurs later and stratification breaks up earlier in fall. On average, the duration of summer-time thermal stratification is now two weeks shorter compared to the conditions that existed before the Project. The results of the Pre-dam ensemble also suggest the lake could have been stratified even before vertical temperature gradients developed, due to a higher content of suspended solids in the JF river. Unfortunately, there are no available in-lake measurements of C_{SS} to confirm this. In general, the changes in the thermal dynamics of Lake Lagarfljót caused by the Project are opposite to those expected from climate warming. For example, reported changes in lake phenology driven by climate warming include longer stratified periods, with earlier onsets of stratification and delayed fall mixing (e.g, Ficker et al., 2017; Niedrist et al., 2018; Woolway et al., 2021). Climate warming has also been shown to lead to an increase in mean annual and/or summer temperature in surface layers (Ficker et al., 2017; Lehnherr et al., 2018; Noori et al., 2022a, 2022b; O'Reilly et al., 2015; Zhang et al., 2014). In their analysis of in-situ and satellite data of 235 lakes distributed worldwide, O'Reilly et al. (2015) found a global warming trend of lake summer surface water temperature LSSWT of + 0.34 °C per decade for the period 1985–2009. This average trend increased to + 0.48 °C per decade when they restricted the analysis to lakes with cold winters (mean winter air temperature < -0.4 °C), as is the case with Lake Lagarfljót. However, in-situ measurements of LSSWT in Lake Lagarfjlót from 2000 to 2015 display a cooling trend of −1.66 °C per decade (Table 1, Fig. S2), potentially counteracting ≈ 4.5 decades of average surface water climate warming occurring in cold lakes. Significant cooling trends have been also observed, for example, in the water surface of lakes in the Tibetan Plateau, which Zhang et al. (2014) linked to increased cold water discharges from accelerated glacier/snow melts.

With some exceptions (e.g., Stetler et al., 2021), a generalized increase in the strength of stratification has been identified in lakes worldwide (e.g., Coats et al., 2006; Ficker et al., 2017; Niedrist et al., 2018; Noori et al., 2022b). Future projections of the thermal structure of lakes, constructed with one-dimensional modeling tools, predict a generalized decrease in the future mixing frequency of lakes at regional (e.g., Råman Vinnå et al., 2021) and global (e.g., Woolway and Merchant, 2019) scales as a result of climate change. As an example, Schwefel et al. (2016) showed that under different climate-change scenarios, the annual mean stability of the water column in the temperate Lake Geneva (Switzerland) could increase up to 21 %. In contrast, this study shows that the annual mean water column stability decreased ≈ 45 % post-dam in Lake Lagarfljót (Fig. 6). This disparate behavior is partially explained by the fact that modeling approaches to analyze the impact of climate change on the thermal structure of lakes at global and regional scales (e.g., Råman Vinnå et al., 2021; Woolway and Merchant, 2019) and international frameworks such as the international ISIMIP Lake Sector framework (Golub et al., 2022) have so far not accounted for inflows/outflows in their projections. This study on a sub-arctic lake adds to other studies in low residence-time lakes with large river–lake temperature differences in temperate (e.g., Carmack et al., 1979; Råman Vinnå et al., 2018) and tropical (e.g., Posada-Bedoya et al., 2021) regions, stressing the importance of accounting for lake tributaries and alterations in the lake catchment in the heat balance and overall thermal structure of lakes.

7. Conclusions

Hydroelectric projects have the potential to introduce significant changes in the stratification and the thermal dynamics of downstream lakes and water bodies. Sub-arctic lakes, characterized by low water column stability, could be particularly sensitive to such projects. Evaluating the impact of hydroelectric projects retrospectively, once they are already built, often faces the challenge of limited or even absent in-lake measurement data prior to the intervention. Even if such data exists, identifying and attributing the observed changes to the range of alterations introduced by these projects or other disturbances (such as interannual and long-term climate changes) can be challenging. In our analysis, we utilized historical data to identify significant changes caused by the hydroelectric project in the lake's hydrological forcing. We proposed a robust approach, based on the analysis of lake forcing, to deconstruct pre-dam conditions from post-dam (actual) conditions through modeling. We also incorporated sources of uncertainty in our dataset. Our findings demonstrate that the hydroelectric project resulted in abrupt changes in the natural hydrological forcing of Lake Lagarfljót, subsequently impacting its summer thermal dynamics. Although our study focuses on Lake Lagarfljót and the Kárahnjúkar Hydroelectric Project in NE Iceland, the results have broader methodological relevance

and implications for analyzing temporal changes in lake thermal dynamics. The modeling approach we employed to assess and comprehend the project's impact, which involves step-by-step deconstruction from post- to pre-operational conditions and considers uncertainty in the hydrological forcing, can be applied to other lakes and existing projects with limited pre-operational in-situ data. Furthermore, our results emphasize the importance of accounting for heat sources/sinks from tributaries when attempting to understand observed changes in lake phenology and thermal stratification. These contributions can potentially mask the effects of other disturbances, such as climate warming.

CRediT authorship contribution statement

Cintia L. Ramón: Conceptualization, Methodology, Formal analysis, Investigation, Writing – original draft, Writing – review & editing. **Francisco J. Rueda:** Writing – review & editing, Writing – original draft, Investigation, Conceptualization. **Morgane C. Priet-Mahéo:** Writing – original draft, Investigation, Data curation. **Hrund Andradóttir:** Writing – review & editing, Writing – original draft, Project administration, Investigation, Funding acquisition, Conceptualization.

Declaration of competing interest

The authors declare that they have no known competing financial interests or personal relationships that could have appeared to influence the work reported in this paper.

Data availability

Data will be made available on request.

Acknowledgments

This work has been founded by the Landsvirkjun Energy Research Fund (Icelandic: Orkurannsóknasjóður Landsvirkjunar) [grant numbers NÝR-02-2016, NÝR-08-2017 and NÝR-11-2018]. Funding for the open-access charge was provided by the University of Granada/CBUA. The Icelandic Meteorological Office and Landsvirkjun are thanked for data access. Special thanks to Hákon Aðalsteinsson for his input to the project. We thank the two anonymous reviewers for their thorough comments and suggestions.

References

Acosta, M., Anguita, M., Rueda, F.J., Fernández-Valdomero, F., 2010. Parallel implementation of a semi-implicit 3D lake hydrodynamic model, in. In: Proceedings of the International Conference on Computational and Mathematical Methods in Science and Engineering, pp. 1026–1037.

Aðalsteinsson, H., 2017. Kárahnjúkavirkjun framkvæmd skilyrða fyrir virkjunarleyfi. Report Number LV-2017-024. Landsvirkjun (in Icelandic).

Aðalsteinsson, H., Böðvarsdóttir, E.B., 2014. Endurmat á gegnsæi í Lagarfljóti fyrir og eftir gangsetningu Kárahnjúkavirkunar. Landsvirkjun (in Icelandic), Reykjavik. Report number LV-2014-074.

Anselmetti, F.S., Bühler, R., Finger, D., Girardclos, S., Lancini, A., Rellstab, C., Sturm, M., 2007. Effects of Alpine hydropower dams on particle transport and lacustrine sedimentation. Aquat. Sci. 69, 179–198. https://doi.org/10.1007/s00027-007-0875-4.

Bermúdez, M., Cea, L., Puertas, J., Rodríguez, N., Baztán, J., 2018. Numerical modeling of the impact of a pumped-storage hydroelectric power plant on the reservoirs' thermal stratification structure: a case study in NW Spain. Environ. Model. Assess. 23, 71–85. https://doi.org/10.1007/S10666-017-9557-3.

Bonalumi, M., Anselmetti, F.S., Kaegi, R., Wüest, A., 2011. Particle dynamics in high-Alpine proglacial reservoirs modified by pumped-storage operation. Water Resour. Res. 47, 9523. https://doi.org/10.1029/2010WR010262.

Bonalumi, M., Anselmetti, F.S., Wüest, A., Schmid, M., 2012. Modeling of temperature and turbidity in a natural lake and a reservoir connected by pumped-storage operations. Water Resour. Res. 48 https://doi.org/10.1029/2012WR011844.

Burkey, J., 2023. Mann-Kendall Tau-b with Sen's Method (enhanced) (https://www.mathworks.com/matlabcentral/fileexchange/11190-mann-kendall-tau-b-with-sen-s-method-enhanced), MATLAB Central File Exchange. Downloaded on February 8, 2023.

Carmack, E.C., Gray, C.B.J., Pharo, C.H., Daley, R.J., 1979. Importance of lake-river interaction on seasonal patterns in the general circulation of Kamloops Lake, British Columbia. Limnol. Oceanogr. 24, 634–644. https://doi.org/10.4319/lo.1979.24.4.0634.

Chen, P., Li, L., Zhang, H., 2016. Spatio-temporal variability in the thermal regimes of the Danjiangkou reservoir and its downstream river due to the large water diversion project system in central China. Hydrol. Res. 47, 104–127. https://doi.org/10.2166/NH.2015.210.

Coats, R., Perez-Losada, J., Schladow, G., Richards, R., Goldman, C., 2006. The warming of Lake Tahoe. Clim. Change 76, 121–148. https://doi.org/10.1007/S10584-005-9006-1.

Dai, Z., Du, J., Li, J., Li, W., Chen, J., 2008. Runoff characteristics of the Changjiang River during 2006: effect of extreme drought and the impounding of the three gorges dam. Geophys. Res. Lett. 35, n/a-n/a. https://doi.org/10.1029/2008GL033456.

De Senerpont Domis, L.N., Elser, J.J., Gsell, A.S., Huszar, V.L.M., Ibelings, B.W., Jeppesen, E., Kosten, S., Mooij, W.M., Roland, F., Sommer, U., Van Donk, E., Winder, M., Lürling, M., 2013. Plankton dynamics under different climatic conditions in space and time. Freshw. Biol. 58, 463–482. https://doi.org/10.1111/FWB.12053.

Denton, F., Halsnæs, K., Akimoto, K., Burch, S., Morejon, C.D., Farias, F., Jupesta, J., Shareef, A., Schweizer-Ries, P., Teng, F., Zusman, E., 2022. Accelerating the transition in the context of sustainable development. In IPCC, 2022: Climate Change 2022: Mitigation of Climate Change. Contribution of Working Group III to the Sixth Assessment Report of the Intergovernmental Panel on Climate Change, in: P.R. Shukla, J. Skea, R. Slade, A. Al Khourdajie, R. van Diemen, D.M., M. Pathak, S. Some, P. Vyas, R. Fradera, M. Belkacemi, A. Hasija, G. Lisboa, S. Luz, J.M. (Eds.), . Cambridge University Press, Cambridge, UK and New York, NY, USA. doi:10.1017/9781009157926.019.

Durran, D.R., 1999. Numerical methods for wave equations in geophysical fluid dynamics, 1st, Editio. ed. Springer-Verlag, New York.

Eiriksdottir, E.S., Oelkers, E.H., Hardardottir, J., Gislason, S.R., 2017. The impact of damming on riverine fluxes to the ocean: a case study from eastern Iceland. Water Res. 113, 124–138. https://doi.org/10.1016/J.WATRES.2016.12.029.

Engelhardt, C., Kirillin, G., 2014. Criteria for the onset and breakup of summer lake stratification based on routine temperature measurements. Fundam. Appl. Limnol. 184, 183–194. https://doi.org/10.1127/1863-9135/2014/0582.

Ficker, H., Luger, M., Gassner, H., 2017. From dimictic to monomictic: empirical evidence of thermal regime transitions in three deep alpine lakes in Austria induced by climate change. Freshw. Biol. 62, 1335–1345. https://doi.org/10.1111/FWB.12946.

Finger, D., Schmid, M., Wüest, A., 2006. Effects of upstream hydropower operation on riverine particle transport and turbidity in downstream lakes. Water Resour. Res. 42, n/a-n/a. https://doi.org/10.1029/2005WR004751.

Fink, G., Wessels, M., Wüest, A., 2016. Flood frequency matters: why climate change degrades deep-water quality of peri-alpine lakes. J. Hydrol. 540, 457–468. https://doi.org/10.1016/j.jhydrol.2016.06.023.

Golub, M., Thiery, W., Marcé, R., Pierson, D., Vanderkelen, I., Mercado-Bettin, D., Woolway, R.I., Grant, L., Jennings, E., Kraemer, B.M., Schewe, J., Zhao, F., Frieler, K., Mengel, M., Bogomolov, V.Y., Bouffard, D., Côté, M., Couture, R.-M., Debolskiy, A.V., Droppers, B., Gal, G., Guo, M., Janssen, A.B.G., Kirillin, G., Ladwig, R., Magee, M., Moore, T., Perroud, M., Piccolroaz, S., Raaman Vinnaa, L., Schmid, M., Shatwell, T., Stepanenko, V.M., Tan, Z., Woodward, B., Yao, H., Adrian, R., Allan, M., Anneville, O., Arvola, L., Atkins, K., Boegman, L., Carey, C., Christianson, K., de Eyto, E., DeGasperi, C., Grechushnikova, M., Hejzlar, J., Joehnk, K., Jones, I.D., Laas, A., Mackay, E.B., Mammarella, I., Markensten, H., McBride, C., Özkundakci, D., Potes, M., Rinke, K., Robertson, D., Rusak, J.A., Salgado, R., van der Linden, L., Verburg, P., Wain, D., Ward, N.K., Wollrab, S., Zdorovennova, G., 2022. A framework for ensemble modelling of climate change impacts on lakes worldwide: the ISIMIP Lake Sector. Geosci. Model Dev. 15, 4597–4623. https://doi.org/10.5194/gmd-15-4597-2022. https://gmd.copernicus.org/articles/15/4597/2022/.

Gross, E., Koseff, J., Monismith, S., 1999. Three-dimensional salinity simulations of South San Francisco Bay. J. Hydraul. Eng. 125, 1199–1209. https://doi.org/10.1061/(ASCE)0733-9429(1999)125:11(1199).

Idso, S.B., 1973. On the concept of lake stability. Limnol. Oceanogr. 18, 681–683. https://doi.org/10.4319/lo.1973.18.4.0681.

Ito, Y., Momii, K., 2015. Impacts of regional warming on long-term hypolimnetic anoxia and dissolved oxygen concentration in a deep lake. Hydrol. Process. 29, 2232–2242. https://doi.org/10.1002/HYP.10362.

Jane, S.F., Hansen, G.J.A., Kraemer, B.M., Leavitt, P.R., Mincer, J.L., North, R.L., Pilla, R. M., Stetler, J.T., Williamson, C.E., Woolway, R.I., Arvola, L., Chandra, S., DeGasperi, C.L., Diemer, L., Dunalska, J., Erina, O., Flaim, G., Grossart, H.P., Hambright, K.D., Hein, C., Hejzlar, J., Janus, L.L., Jenny, J.P., Jones, J.R., Knoll, L. B., Leoni, B., Mackay, E., Matsuzaki, S.I.S., McBride, C., Müller-Navarra, D.C., Paterson, A.M., Pierson, D., Rogora, M., Rusak, J.A., Sadro, S., Saulnier-Talbot, E., Schmid, M., Sommaruga, R., Thiery, W., Verburg, P., Weathers, K.C., Weyhenmeyer, G.A., Yokota, K., Rose, K.C., 2021. Widespread deoxygenation of temperate lakes. Nature 594, 66–70. https://doi.org/10.1038/s41586-021-03550-y.

Kantha, L.H., Clayson, C.A., 1994. An improved mixed layer model for geophysical applications. J. Geophys. Res. Ocean. 99, 25235–25266. https://doi.org/10.1029/94JC02257.

Kobler, U., Wüest, A., Schmid, M., 2018. Effects of Lake-reservoir pumped-storage operations on temperature and water quality. Sustainability 10, 1968. https://doi.org/10.3390/su10061968.

Kondo, J., 1975. Air-sea bulk transfer coefficients in diabatic conditions. Boundary-Layer Meteorol. 9, 91–112. https://doi.org/10.1007/BF00232256.

Lehnherr, I., St Louis, V.L., Sharp, M., Gardner, A.S., Smol, J.P., Schiff, S.L., Muir, D.C.G., Mortimer, C.A., Michelutti, N., Tarnocai, C., St Pierre, K.A., Emmerton, C.A., Wiklund, J.A., Köck, G., Lamoureux, S.F., Talbot, C.H., 2018. The world's largest High Arctic lake responds rapidly to climate warming. Nat. Commun. 2018 91 9, 1–9. doi:10.1038/s41467-018-03685-z.

Lessard, J.L., Hayes, D.B., 2003. Effects of elevated water temperature on fish and macroinvertebrate communities below small dams. River Res. Appl. 19, 721–732. https://doi.org/10.1002/rra.713.

Loizeau, J.-L., Dominik, J., 2000. Evolution of the upper Rhone River discharge and suspended sediment load during the last 80 years and some implications for Lake Geneva. Aquat. Sci. 62, 54–67. https://doi.org/10.1007/s000270050075.

Lu, G., Wells, M., van Strygen, I., Hecky, R.E., 2022. Intrusions of sediment laden rivers into density stratified water columns could be an unrecognized source of mixing in many lakes and coastal oceans. Sedimentology 69, 2228–2245. https://doi.org/10.1111/SED.12990.

Maavara, T., Chen, Q., Van Meter, K., Brown, L.E., Zhang, J., Ni, J., Zarfl, C., 2020. River dam impacts on biogeochemical cycling. Nat. Rev. Earth Environ. 2020 12 1, 103–116. doi:10.1038/s43017-019-0019-0.

Martin, J.L., McCutcheon, S.C., 1999. Hydrodynamics and transport for water quality modeling. CRC Press, Boca Ratón, Florida.

McKay, M.D., Beckman, R.J., Conover, W.J., 1979. Comparison of three methods for selecting values of input variables in the analysis of output from a computer code. Technometrics 21, 239–245. https://doi.org/10.1080/00401706.1979.10489755.

Mellor, G.L., Yamada, T., 1974. A Hierarchy of turbulence closure models for Planetary Boundary layers. J. Atmos. Sci. 31, 1791–1806. https://doi.org/10.1175/1520-0469(1974)031<1791:AHOTCM>2.0.CO;2.

Niedrist, G.H., Psenner, R., Sommaruga, R., 2018. Climate warming increases vertical and seasonal water temperature differences and inter-annual variability in a mountain lake. Clim. Change 151, 473–490. https://doi.org/10.1007/S10584-018-2328-6.

Noori, R., Bateni, S.M., Saari, M., Almazroui, M., Torabi Haghighi, A., 2022a. Strong Warming rates in the Surface and bottom layers of a boreal Lake: results from approximately six decades of measurements (1964–2020). e2021EA001973 Earth Sp. Sci. 9. https://doi.org/10.1029/2021EA001973.

Noori, R., Woolway, R.I., Saari, M., Pulkkanen, M., Kløve, B., 2022b. Six decades of thermal change in a pristine Lake situated north of the Arctic circle. e2021WR031543 Water Resour. Res. 58. https://doi.org/10.1029/2021WR031543.

O'Reilly, C.M., Sharma, S., Gray, D.K., Hampton, S.E., Read, J.S., Rowley, R.J., Schneider, P., Lenters, J.D., McIntyre, P.B., Kraemer, B.M., Weyhenmeyer, G.A., Straile, D., Dong, B., Adrian, R., Allan, M.G., Anneville, O., Arvola, L., Austin, J., Bailey, J.L., Baron, J.S., Brookes, J.D., De Eyto, E., Dokulil, M.T., Hamilton, D.P., Havens, K., Hetherington, A.L., Higgins, S.N., Hook, S., Izmest'Eva, L.R., Joehnk, K. D., Kangur, K., Kasprzak, P., Kumagai, M., Kuusisto, E., Leshkevich, G., Livingstone, D.M., MacIntyre, S., May, L., Melack, J.M., Mueller-Navarra, D.C., Naumenko, M., Noges, P., Noges, T., North, R.P., Plisnier, P.D., Rigosi, A., Rimmer, A., Rogora, M., Rudstam, L.G., Rusak, J.A., Salmaso, N., Samal, N.R., Schindler, D.E., Schladow, S. G., Schmid, M., Schmidt, S.R., Silow, E., Soylu, M.E., Teubner, K., Verburg, P., Voutilainen, A., Watkinson, A., Williamson, C.E., Zhang, G., 2015. Rapid and highly variable warming of lake surface waters around the globe. Geophys. Res. Lett. 42, 10,773-10,781. doi:10.1002/2015GL066235.

Posada-Bedoya, A., Gómez-Giraldo, A., Román-Botero, R., 2021. Effects of riverine inflows on the climatology of a tropical andean reservoir. Limnol. Oceanogr. lno.11897 https://doi.org/10.1002/lno.11897.

Prats, J., Val, R., Armengol, J., Dolz, J., 2010. Temporal variability in the thermal regime of the lower Ebro River (Spain) and alteration due to anthropogenic factors. J. Hydrol. 387, 105–118. https://doi.org/10.1016/j.jhydrol.2010.04.002.

Preece, R.M., Jones, H.A., 2002. The effect of keepit dam on the temperature regime of the Namoi River. Australia. River Res. Appl. 18, 397–414. https://doi.org/10.1002/rra.686.

Priet-Mahéo, M.C., 2019. Internal dynamics of a medium-sized subarctic lake: field measurements and numerical modeling. University of Iceland.

Priet-Mahéo, M.C., Ramón, C.L., Rueda, F.J., Andradóttir, H.Ó., 2019. Mixing and internal dynamics of a medium-size and deep lake near the Arctic circle. Limnol. Oceanogr. 64, 61–80. https://doi.org/10.1002/lno.11019.

Råman Vinnå, L., Wüest, A., Zappa, M., Fink, G., Bouffard, D., 2018. Tributaries affect the thermal response of lakes to climate change. Hydrol. Earth Syst. Sci. 22, 31–51. https://doi.org/10.5194/hess-22-31-2018.

Råman Vinnå, L., Medhaug, I., Schmid, M., Bouffard, D., 2021. The vulnerability of lakes to climate change along an altitudinal gradient. Commun. Earth Environ. 2, 1–10. https://doi.org/10.1038/s43247-021-00106-w.

Ramón, C.L., Priet-Mahéo, M.C., Rueda, F.J., Andradóttir, H., 2020. Inflow dynamics in weakly Stratified Lakes subject to Large isopycnal displacements. e2019WR026578 Water Resour. Res. 56. https://doi.org/10.1029/2019WR026578.

Schwefel, R., Gaudard, A., Wüest, A., Bouffard, D., 2016. Effects of climate change on deepwater oxygen and winter mixing in a deep lake (Lake Geneva): Comparing observational findings and modeling. Water Resour. Res. 52, 8811–8826. https://doi.org/10.1002/2016WR019194.

Smith, P., 2006. A semi-implicit, three-dimensional model of Estuarine circulation. USGS, Sacramento, USA. Open File Report 2006–1004,.

Stetler, J.T., Girdner, S., Mack, J., Winslow, L.A., Leach, T.H., Rose, K.C., 2021. Atmospheric stilling and warming air temperatures drive long-term changes in lake stratification in a large oligotrophic lake. Limnol. Oceanogr. 66, 954–964. https://doi.org/10.1002/lno.11654.

Striberger, J., Björck, S., Ingólfsson, Ó., Kjær, K.H., Snowball, I., Uvo, C.B., 2011. Climate variability and glacial processes in eastern Iceland during the past 700 years based on varved lake sediments. Boreas 40, 28–45. https://doi.org/10.1111/J.1502-3885.2010.00153.X.

Valerio, G., Pilotti, M., Barontini, S., Leoni, B., 2015. Sensitivity of the multiannual thermal dynamics of a deep pre-alpine lake to climatic change. Hydrol. Process. 29, 767–779. https://doi.org/10.1002/HYP.10183.

Wells, M.G., Wettlaufer, J.S., 2007. The long-term circulation driven by density currents in a two-layer stratified basin. J. Fluid Mech. 572, 37. https://doi.org/10.1017/S0022112006003478.

Wetzel, R.G., 2001. Limnology: Lake and river ecosystems, Third. ed. Academic Press, San Diego. doi:10.1016/C2009-0-02112-6.

Winton, R.S., Calamita, E., Wehrli, B., 2019. Reviews and syntheses: dams, water quality and tropical reservoir stratification. Biogeosciences 16, 1657–1671. https://doi.org/10.5194/BG-16-1657-2019.

Woolway, R.I., Merchant, C.J., 2019. Worldwide alteration of lake mixing regimes in response to climate change. Nat. Geosci. 12, 271–276. https://doi.org/10.1038/s41561-019-0322-x.

Woolway, R.I., Sharma, S., Weyhenmeyer, G.A., Debolskiy, A., Golub, M., Mercado-Bettín, D., Perroud, M., Stepanenko, V., Tan, Z., Grant, L., Ladwig, R., Mesman, J., Moore, T.N., Shatwell, T., Vanderkelen, I., Austin, J.A., DeGasperi, C.L., Dokulil, M., La Fuente, S., Mackay, E.B., Schladow, S.G., Watanabe, S., Marcé, R., Pierson, D.C., Thiery, W., Jennings, E., 2021. Phenological shifts in lake stratification under climate change. Nat. Commun. 12, 2318. https://doi.org/10.1038/s41467-021-22657-4.

Wüest, A., Imboden, D.M., Schurter, M., 1988. Origin and size of hypolimnic mixing in urnersee, the southern basin of vierwaldstättersee (Lake Lucerne). Swiss J. Hydrol. 50, 40–70. https://doi.org/10.1007/BF02538371.

Yang, S.L., Zhang, J., Xu, X.J., 2007. Influence of the three gorges dam on downstream delivery of sediment and its environmental implications, Yangtze River. Geophys. Res. Lett. 34, n/a-n/a. https://doi.org/10.1029/2007GL029472.

Yankova, Y., Villiger, J., Pernthaler, J., Schanz, F., Posch, T., 2016. Prolongation, deepening and warming of the metalimnion change habitat conditions of the harmful filamentous cyanobacterium Planktothrix rubescens in a prealpine lake. Hydrobiologia 776, 125–138. https://doi.org/10.1007/s10750-016-2745-3.

Zhang, C., Fujiwara, M., Pawluk, M., Liu, H., Cao, W., Gao, X., 2020. Changes in taxonomic and functional diversity of fish communities after catastrophic habitat alteration caused by construction of three gorges dam. Ecol. Evol. 10, 5829–5839. https://doi.org/10.1002/ECE3.6320.

Zhang, R., Wu, B., 2020. Environmental impacts of high water turbidity of the Niulan River to dianchi Lake water diversion project. J. Environ. Eng. 146, 05019006. https://doi.org/10.1061/(ASCE)EE.1943-7870.0001623.

Zhang, G., Yao, T., Xie, H., Qin, J., Ye, Q., Dai, Y., Guo, R., 2014. Estimating surface temperature changes of lakes in the tibetan plateau using MODIS LST data. J. Geophys. Res. Atmos. 119, 8552–8567. https://doi.org/10.1002/2014JD021615.

Zhao, K., Wulder, M.A., Hu, T., Bright, R., Wu, Q., Qin, H., Li, Y., Toman, E., Mallick, B., Zhang, X., Brown, M., 2019. Detecting change-point, trend, and seasonality in satellite time series data to track abrupt changes and nonlinear dynamics: a bayesian ensemble algorithm. Remote Sens. Environ. 232, 111181 https://doi.org/10.1016/J.RSE.2019.04.034.